Boundary curvature effect on the wrinkling of thin suspended films

Applied Physics Letters

Boundary curvature effect on the wrinkling of thin suspended films

Cite as: Appl. Phys. Lett. **116**, 193702 (2020); https://doi.org/10.1063/5.0006164
Submitted: 28 February 2020 . Accepted: 15 April 2020 . Published Online: 11 May 2020

Stoffel D. Janssens, Burhannudin Sutisna, Alessandro Giussani, James A. Kwiecinski, David Vázquez-Cortés, and Eliot Fried

Applied Physics Letters ARTICLE scitation.org/journal/apl

Boundary curvature effect on the wrinkling of thin suspended films

Cite as: Appl. Phys. Lett. **116**, 193702 (2020); doi: 10.1063/5.0006164
Submitted: 28 February 2020 · Accepted: 15 April 2020 ·
Published Online: 11 May 2020

Stoffel D. Janssens, Burhannudin Sutisna, Alessandro Giussani, James A. Kwiecinski, David Vázquez-Cortés, and Eliot Fried[a)]

AFFILIATIONS

Mathematics, Mechanics, and Materials Unit (MMMU), Okinawa Institute of Science and Technology Graduate University (OIST), 1919-1 Tancha, Onna-son, Kunigami-gun, Okinawa 904-0495, Japan

[a)]Author to whom correspondence should be addressed: eliot.fried@oist.jp. URL: https://groups.oist.jp/mmmu

ABSTRACT

A relation between the boundary curvature κ and the wrinkle wavelength λ of a thin suspended film under boundary confinement is demonstrated. Experiments were performed with nanocrystalline diamond films of approximate thickness 184 nm grown on glass substrates. By removing portions of the substrates after growth, suspended films with circular boundaries of radius 30–811 μm were fabricated. Due to residual stresses, the portions of the film bonded to the substrate are of approximate compressive prestrain 11×10^{-4} and the suspended portions of the film are azimuthally wrinkled at their boundary. Measurements show that λ decreases monotonically with κ, and a simple model that is in line with this trend is proposed. The model can be applied to design devices with functional wrinkles and can be adapted to gain insight into other systems such as plant leaves. A method for measuring residual compressive strain in thin films, which complements standard strain characterization methods, is also described.

Wrinkling is an ubiquitous natural phenomenon and has fostered the evolution of tissue that lowers the expenditure of energy.[1,2] Recently, wrinkling has been explored to design efficient devices with self-similar patterns, such as vibration energy harvesters,[3] solar cells,[4] and light gratings.[5,6] However, wrinkling is also known to have adverse effects on the operation of devices such as pressure sensors.[7] The omnipresence of wrinkling strongly motivates us to understand this phenomenon. Thin films are known to wrinkle because of excess area and geometric compaction,[8,9] and are typically modeled using the Föppl–von Kármán theory of plates in conjunction with scaling arguments and asymptotic analysis. The characteristic wrinkle wavelength λ of a thin film is found by minimizing energy and is provided by the scaling relation

$$\lambda \sim \frac{t^{1/2}}{\varepsilon^{1/4}}, \tag{1}$$

where t is the film thickness and ε is a strain that induces wrinkling.[10–12] Efforts to investigate the effect of the boundary curvature on the wrinkling of thin films began only recently. Experiments and simulations have shown that curvature can significantly affect the wrinkling of cylindrical shells upon stretching.[13] For spherical[14,15] or tubular[16,17] bilayer systems, similar conclusions have been reached.

Here, we present experiments showing that the boundary curvature of a thin suspended film has a relatively strong impact on azimuthal wrinkling. We provide a model that confirms this finding and can be used to design devices with functional wrinkles. The model hinges on the assumption that the film is composed of a mechanically isotropic material. This assumption is often made to simplify the deformation analysis of 2D materials, amorphous materials, and single crystals, which suggests that the model can be widely applied. We also present a method, which complements those recently reviewed,[18] for measuring the residual compressive strain and film area density from the height profile of a suspended film.

The results are obtained from systematic experiments performed with suspended nanocrystalline diamond (NCD) films of average thickness $t = 184 \pm 9$ nm, nearly circular boundaries of radius R ranging from 30 to 811 μm, and a compressive prestrain of $\varepsilon_0 \approx 11 \times 10^{-4}$, which prevails at and beyond the boundaries where the film is bonded to the substrate. A reflecting optical microscope image of such a film is shown in Fig. 1. The films were grown on glass substrates, after which circular portions of the substrates were removed by etching. Each film consists of portions that are bonded to the substrate and free-standing portions. The bonded and free-standing portions of each film are

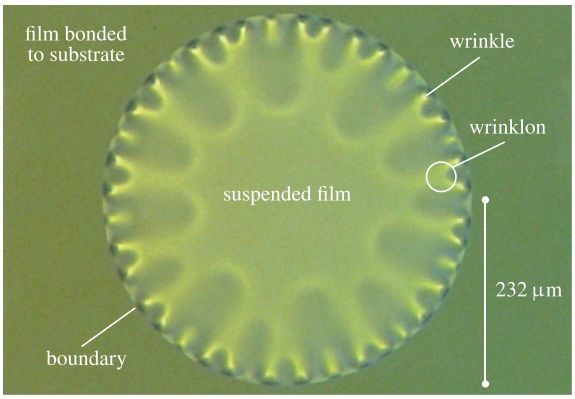

FIG. 1. Reflecting optical microscope image of a continuous nanocrystalline diamond (NCD) film of approximate thickness $t = 184$ nm, which was grown on a glass substrate. The suspended portion of the film has a circular boundary of radius $R = 232$ μm and was made by etching the substrate from the backside. Due to residual stresses, the portion of the film bonded to the substrate is of compressive prestrain $\varepsilon_0 \approx 11 \times 10^{-4}$ and the suspended portion of the film, which remains contiguously connected to the bonded film, is azimuthally wrinkled. The compressive strain in the suspended portion of the film relaxes toward its center. A wrinklon, which is indicated by the circle, is the localized transition zone in the merging of two wrinkles.[19]

contiguously connected. Due to residual compressive stresses in the bonded portions of the film and the presence of boundary confinement, excess area is formed and geometric compaction occurs in the suspended films. The compressive strain in these films is relaxed radially by buckling and azimuthally by wrinkling. Experimental details are provided hereinafter. In contrast to ultra-thin polymer films,[20] NCD films can be regarded to be elastic. The prestrain ε_0 is, therefore, time-invariant so that the wrinkling and underlying strain of the films can be characterized in detail. Another reason for using the suspended NCD films supported by glass substrates is that they are promising candidates for use as robust pressure sensors[7,21] and for the development of 3D micro- and nanodevices.[22]

From the experiments described hereinafter, we find that λ monotonically decreases with boundary curvature $\kappa = 1/R$. To explain this trend, we present a model involving a penetration depth ΔR over which strain in the suspended film relaxes. Only positive compressive strains are considered in the experimental aspects of this work. The setup of our problem is depicted in Fig. 2(a), where ΔR and all other salient geometrical quantities entering our formulation are described. For convenience, the symbols used in this work, and their description, are listed in Table I. We assume that the radial strain ε_{rr} is independent of the hoop strain $\varepsilon_{\theta\theta}$; the shear strain $\varepsilon_{r\theta}$ vanishes, the film is made of a mechanically isotropic material, and the portion of the film for which $d \geq \Delta R$ undergoes pure bending (i.e., is not subject to stretching). Since wrinkling occurs azimuthally with respect to the origin O, we infer that $\varepsilon = \varepsilon_{\theta\theta}$. On this basis, we find that

$$\varepsilon = \frac{s}{l} - 1 = \frac{s}{\theta(R - \Delta R)} - 1. \tag{2}$$

If the curvature κ of the supporting edge vanishes, as depicted in Fig. 2(b), we find that

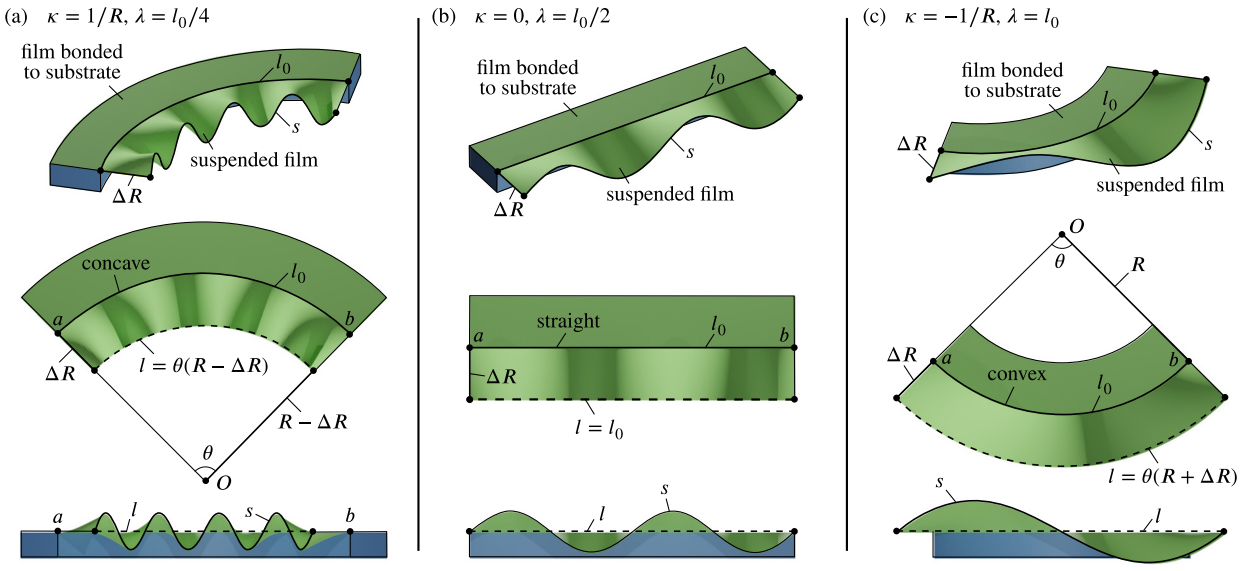

FIG. 2. (a) From top to bottom, with respect to the figure, a bird's-eye view, top view, and side view of a schematic of a continuous portion of film, based on Fig. 1, which assist in describing the model presented in this work. The portion of the film that is bonded to the substrate is subject to a compressive prestrain ε_0, and the suspended film is contiguously connected to the portion of the film that is bonded to the substrate. The length of a portion of boundary is denoted by l_0 and the penetration depth ΔR is on the order of the length over which strain in the suspended film relaxes. At distance ΔR from the boundary, a curve of arc length l, which is the projection of the oscillating curve of arc length s, exists. The projection is done from the suspended film, which is of radius R, to the plane $\mathscr{P}$, which is defined by points a, O, and b. Within $\mathscr{P}$, a polar coordinate system with origin O, radial coordinate r, and azimuthal angle θ is defined. The radial distance d is measured from the boundary to O. With respect to the top view schematic, the boundary is concave and has a signed curvature $\kappa = 1/R$ that is arbitrarily chosen to be positive. (b) and (c) are cases for which the boundary is straight, so that $\kappa = 0$, and convex, so that $\kappa = -1/R$, respectively. The effect of κ on wrinkle wavelength λ is illustrated by increasing λ monotonically from (a) to (c).

TABLE I. List of symbols with description.

A	Surface area of a suspended film
A_i	Area of a surface triangle T_i
B	Bending stiffness of a cantilever
c	Proportionality constant of Eq. (6)
d	Radial distance measured from the boundary of a suspended film to origin O
$\mathscr{D}$	Dimensional number that compares S with B
E	Young's modulus
l	Arc length of the curve that is the projection on plane $\mathscr{P}$ of the curve of arc length s
l_0	Arc length of a portion of boundary
O	Origin of the polar coordinate system in plane $\mathscr{P}$
P_i	Area of the projection of T_i on $\mathscr{P}$
$\mathscr{P}$	Plane defined by points a, O, and b in Fig. 2
r	Radial coordinate of the polar coordinate system in plane $\mathscr{P}$
R	Radius of the boundary of a suspended film
s	Arc length of the oscillating curve at $d = \Delta R$
S	Stretching stiffness of a cantilever
t	Thickness of a film
T_i	Surface triangle i of a triangulated surface
w	Width of a cantilever
ΔR	Penetration depth over which the strain in the suspended portion of film relaxes
ζ	Approximate measure for strain
ε	Strain that induces wrinkling
ε_0	Compressive prestrain of the portions of film bonded to the substrate
ε_{rr}	Compressive radial strain
$\varepsilon_{r\theta}$	Compressive shear strain
$\varepsilon_{\theta\theta}$	Compressive hoop strain
θ	Azimuthal angle of the polar coordinate system in plane $\mathscr{P}$
κ	Signed boundary curvature of a suspended film
λ	Wrinkle wavelength

$$\varepsilon = \frac{s}{l} - 1 = \frac{s}{l_0} - 1 = \varepsilon_0. \tag{3}$$

For $\kappa = 1/R$, it can be observed from Fig. 2(a) that $l < l_0$. This shows that geometric compaction occurs when the curvature κ of the supporting edge is positive. If $R \gg \Delta R$, we can apply the binomial theorem to expand $(R - \Delta R)^{-1}$ and write Eq. (2) as

$$\varepsilon \sim \varepsilon_0 + \frac{s}{l_0}\Delta R\kappa. \tag{4}$$

For a small wrinkle amplitude at $d = \Delta R$, the quotient s/l_0 is practically unity and we may write Eq. (4) as

$$\varepsilon \sim \varepsilon_0 + \Delta R\kappa. \tag{5}$$

With Eqs. (1) and (5), we then obtain

$$\lambda \sim \frac{t^{1/2}}{(\varepsilon_0 + \Delta R\kappa)^{1/4}}. \tag{6}$$

For $\kappa = -1/R$, as depicted in Fig. 2(c), Eq. (6) is also obtained using similar arguments as for $\kappa = 1/R$. Given that ΔR and ε_0 are constant, Eq. (6) predicts that λ decreases monotonically with κ. As expected, Eq. (5) reduces to Eq. (3) for $\kappa = 0$. For our problem, Eqs. (1) and (6) are independent of material properties.[10]

To fabricate our films, we first seeded $10 \times 10 \times 0.2$ mm^3 Lotus NXT glass substrates with nanodiamonds.[23,24] Subsequently, a closed film was grown by plasma-assisted chemical vapor deposition in the reactor of an SDS6500X microwave system with 1.5 kW of 2.45 GHz microwaves. During film growth, the substrate temperature was maintained at about 873 K and the reactor was kept at a pressure of 2 kPa with 294 sccm of hydrogen gas and 6 sccm of methane gas. The thicknesses of the NCD films were measured using a Hamamatsu C13027 optical nano gauge. The through holes in the glass substrates and the suspended films were fabricated by etching the substrate locally with hydrofluoric acid using recently described techniques.[21,22] Reflecting optical microscope images and surface profiles of the suspended films were taken using a Keyence VK-X150 confocal laser microscope. We define a surface profile as a collection of heights of a suspended film with reference to plane $\mathscr{P}$. Similar to previous work,[22] film stresses were obtained by X-ray diffraction (XRD) measurements carried out using a Bruker D8 Discover diffractometer.

To estimate the magnitude of ΔR, we use the dimensionless number $\mathscr{D} = S/B$, where S and B denote the stretching and bending stiffness, respectively. In so doing, we assume that a portion of suspended film acts as a cantilever of width w, thickness t, and length d. Then, $S = Etw/d$ and $B = Et^3w/4d^3$, where E denotes Young's modulus, so that $\mathscr{D} = 4(d/t)^2$. For $d = t$, we see that $\mathscr{D} = 4$, which indicates that bending and stretching stiffnesses are of the same order. However, for a relatively small value of d, for example, 2 μm, and $t = 184$ nm, we see that $\mathscr{D} = 473$, which indicates that bending is strongly favorable over stretching. On this basis, we estimate that ΔR is on the order of micrometers, that $R \gg \Delta R$, and that ΔR depends on t. Because t is kept nearly constant in our experiments, the latter dependency is not investigated.

From XRD measurements, we infer that the thermal mismatch between the substrate and the film induces a compressive prestrain with a value of $\varepsilon_0 = (11 \pm 2) \times 10^{-4}$, taking into account that, from a Raman spectroscopy study reported previously,[22] intrinsic strain is known to be negligible. However, when the material properties of a film are unknown or when dealing with ultra-thin films or amorphous materials, other methods are needed to obtain ε_0. To solve this problem, we demonstrate that ε_0 is estimated accurately by

$$\zeta = \sqrt{\frac{A}{\pi R^2}} - 1, \tag{7}$$

where A denotes the surface area of the suspended film. The relation $\varepsilon_0 \sim \zeta$ holds if stretching is negligible, a criterion that is met in our work. The area A of the suspended film is estimated by removing noise from a surface profile with a Gauss filter, creating a surface from that filtered profile by triangulation, calculating the area A_i of each surface triangle T_i, and summing up all A_i that correspond to the suspended film. We find, for our films, that $\varepsilon_0 = (11 \pm 2) \times 10^{-4}$. This value is in excellent agreement with the value obtained from XRD measurements and shows that our approach yields results consistent with a standard strain characterization method. One of the surface profiles used to obtain ε_0 appears in Fig. 3(a), which is for the film shown in Fig. 1. Figure 3(b) depicts $(A_i/P_i) - 1$, as obtained from the height

profile in Fig. 3(a), plotted with respect to $\mathscr{P}$, in which P_i denotes the area of the projection of T_i on $\mathscr{P}$. The ratio A_i/P_i represents the scaled film area density under the assumption that stretching is negligible. From the plot, we observe that A_i/P_i is greater at the wrinkled portion than at the remaining area of the suspended film. This shows that in addition to providing a value for ε_0, our strain analysis is useful for investigating the film area density.

To demonstrate that λ decreases monotonically with κ, three surface profiles of the suspended NCD films taken at $d \approx 6$ μm are given in Fig. 4(a), with a relatively small offset in height for clarity. Accurate values of λ are found by counting the number of wrinkles of a suspended film and dividing the resulting number by $2\pi R$. Counting is most easily done with reflecting optical microscope images, of which one appears in Fig. 1. For that image, 39 ± 1 wrinkles were counted, as confirmed from analyzing height profiles such as those given in Fig. 4(a). In Fig. 4(b), the obtained values of λ, scaled by $t^{1/2}$, are plotted vs κ. To fit the data in Fig. 4(b) with our model, using the least squares method, Eq. (6) is written as

$$\frac{\lambda}{t^{1/2}} = \frac{c}{(\varepsilon_0 + \Delta R\kappa)^{1/4}}, \tag{8}$$

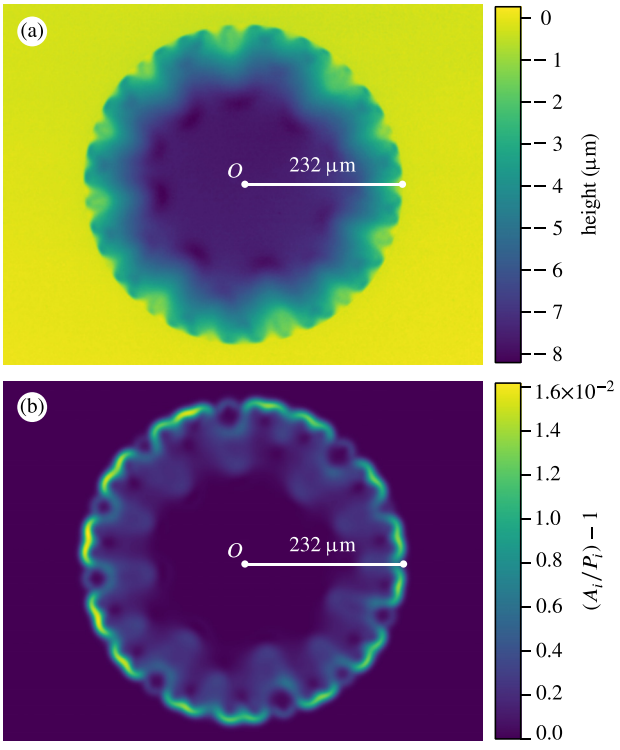

FIG. 3. (a) Surface profile of the suspended film depicted in Fig. 1. From the profile, it is clear that radially the film buckles out of plane $\mathscr{P}$ and azimuthally the film wrinkles. This is one of the profiles used to obtain $\varepsilon_0 = (11 \pm 2) \times 10^{-4}$ with $\varepsilon_0 \sim \sqrt{A/\pi R^2} - 1$. Here, A denotes the surface area of the suspended film, as found by removing noise from a surface profile, creating a surface from that smooth surface profile by triangulation, calculating the area A_i of each triangle T_i, and summing up all A_i that correspond to the suspended film. (b) $(A_i/P_i) - 1$ obtained from (a) plotted with respect to $\mathscr{P}$. Here, P_i denotes the area of the projection of T_i on $\mathscr{P}$. Given that stretching is negligible, A_i/P_i is the scaled film area density. This ratio is the greatest at the wrinkled portion of the suspended film.

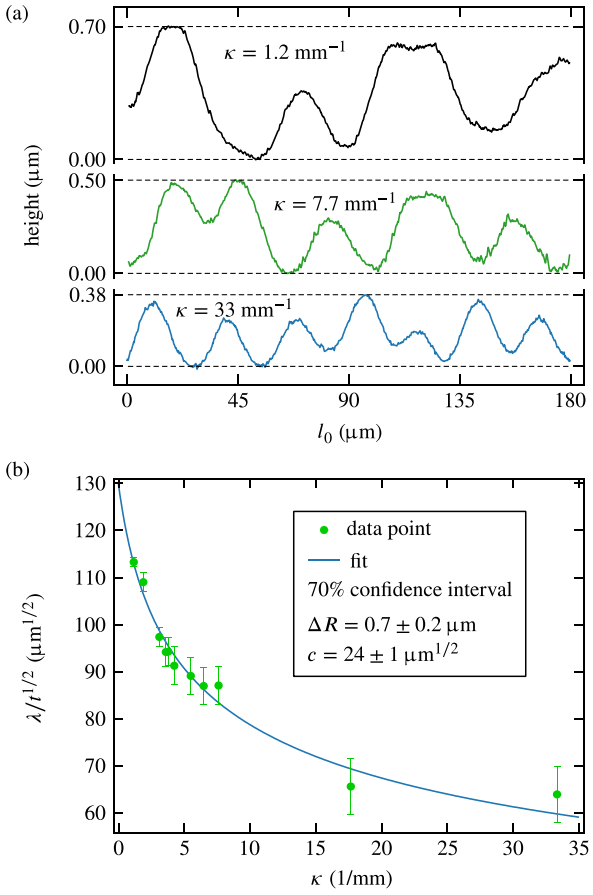

FIG. 4. (a) Surface profiles of the suspended NCD films measured at approximately 6 μm from their boundaries, with respect to $\mathscr{P}$, and plotted vs l_0. A relatively small offset in height is applied for clarity. From these data, we deduce that the wrinkle wavelength λ and wrinkle amplitude decrease monotonically with κ. (b) Wrinkle wavelength λ divided by $t^{1/2}$ vs κ. Eq. (8) is fitted to the data with $\varepsilon_0 = 11 \times 10^{-4}$ and fitting parameters c and ΔR, with c denoting a proportionality constant. This result supports the assertion that our wrinkling model captures the main physical ingredients that explain our observations.

in which $\varepsilon_0 = 11 \times 10^{-4}$, ΔR is assumed to be constant, and ΔR and the proportionality constant c act as fitting parameters. Since Eq. (6) is independent of materials properties, so is Eq. (8). The fit confirms that our wrinkling model captures the main physical ingredients that explain our observations. For a confidence interval of 70%, we find that $c = 24 \pm 1$ μm$^{1/2}$ and $\Delta R = 0.7 \pm 0.2$ μm. These results support the relation $R \gg \Delta R$. Since Eq. (8) is free of materials properties, changes in the material properties of NCD, which are often attributed to the grain size,[25] are assumed not to affect λ.

Under the assumption that stretching is negligible for $d \geq \Delta R$, the arc length of the curves in Fig. 4(a) should be similar, in which case the wrinkle amplitude decreases with λ. This is verified by comparing the height axis of the surface profiles in Fig. 4(a). Further analysis of the wrinkle amplitude vs d may be done within the formalism based on wrinklons,[19] which we leave for future work. A wrinklon is the localized transition zone in the merging of two wrinkles. Such a zone is indicated in Fig. 1.

For a leaf that is supported by a stem of radius R, Xu and coworkers[26] suggest that residual growth strain induces wrinkling of the leaf. Interestingly, they predict that the associated wrinkle wavelength λ decreases monotonically with R. By modeling such a leaf as a thin suspended film supported by a rigid stem of curvature $\kappa = -1/R$, as depicted in Fig. 2(c), and attributing ε_0 to growth, our model provides a similar prediction, given that ΔR and ε_0 are approximately constant. Experimentally, the case $\kappa = -1/R$ may be verified by fabricating micro-disk like structures.[27,28]

To finalize our discussion, we underline that due to the presence of the curvature in our experiments, the wrinkle density is practically doubled. It is, therefore, evident that, apart from dynamic wrinkling,[29] the boundary curvature also needs to be taken into account when designing devices with functional wrinkles.

We conclude that boundary curvature can strongly influence the wrinkling of thin suspended films. Experimentally, we showed this by growing nanocrystalline diamond films of approximate thickness 184 nm on glass substrates. Due to residual stresses, a compressive strain in the films was introduced. By removing portions of the substrate, suspended, azimuthally wrinkled films with circular boundaries of radius 30–811 μm were fabricated. We found that the wavelength of these wrinkles decreases monotonically with the boundary curvature, leading to a doubling of the wrinkle density. A model that is in line with our experiments is provided. This model can be used to design devices with functional wrinkles, is adapted to explain how the radius of a plant stem affects the wrinkling of the leaf that it supports, and may also be adapted to afford insight into other similar systems. Additionally, taking advantage of the fact that for relatively thin suspended films deformation is dominated by bending, meaning that stretching is negligible, we established a method for measuring residual compressive strain and film area density from height profiles. The method complements standard strain characterization methods.

We gratefully acknowledge the support from the Okinawa Institute of Science and Technology Graduate University with subsidy funding from the Cabinet Office, Government of Japan.

The data that support the findings of this study are available from the corresponding author upon reasonable request.

REFERENCES

[1]M. R. Nixon, A. G. Orr, and P. Vukusic, "Wrinkles enhance the diffuse reflection from the dragonfly Rhyothemis resplendens," J. R. Soc. Interface **12**, 20140749 (2015).
[2]A. F. Martins, N. C. Bennett, S. Clavel, H. Groenewald, S. Hensman, S. Hoby, A. Joris, P. R. Manger, and M. C. Milinkovitch, "Locally-curved geometry generates bending cracks in the African elephant skin," Nat. Commun. **9**, 3865 (2018).
[3]A. H. Hosseinloo and K. Turitsyn, "Energy harvesting via wrinkling instabilities," Appl. Phys. Lett. **110**, 013901 (2017).
[4]J. B. Kim, P. Kim, N. C. Pégard, S. J. Oh, C. R. Kagan, J. W. Fleischer, H. A. Stone, and Y.-L. Loo, "Wrinkles and deep folds as photonic structures in photovoltaics," Nat. Photonics **6**, 327–332 (2012).
[5]C. Harrison, C. M. Stafford, W. Zhang, and A. Karim, "Sinusoidal phase grating created by a tunably buckled surface," Appl. Phys. Lett. **85**, 4016–4018 (2004).
[6]F. Li, H. Hou, J. Yin, and X. Jiang, "Near-infrared light–responsive dynamic wrinkle patterns," Sci. Adv. **4**, eaar5762 (2018).
[7]S. Drijkoningen, S. D. Janssens, P. Pobedinskas, S. Koizumi, M. K. Van Bael, and K. Haenen, "The pressure sensitivity of wrinkled b-doped nanocrystalline diamond membranes," Sci. Rep. **6**, 35667 (2016).
[8]J. Huang, B. Davidovitch, C. D. Santangelo, T. P. Russell, and N. Menon, "Smooth cascade of wrinkles at the edge of a floating elastic film," Phys. Rev. Lett. **105**, 038302 (2010).
[9]M. Leocmach, M. Nespoulous, S. Manneville, and T. Gibaud, "Hierarchical wrinkling in a confined permeable biogel," Sci. Adv. **1**, e1500608 (2015).
[10]G. Gioia and M. Ortiz, "Delamination of compressed thin films," Adv. Appl. Mech. **33**, 119–192 (1997).
[11]E. Cerda and L. Mahadevan, "Geometry and physics of wrinkling," Phys. Rev. Lett. **90**, 074302 (2003).
[12]E. Puntel, L. Deseri, and E. Fried, "Wrinkling of a stretched thin sheet," J. Elast. **105**, 137–170 (2011).
[13]T. Wang, Y. Yang, C. Fu, F. Liu, K. Wang, and F. Xu, "Wrinkling and smoothing of a soft shell," J. Mech. Phys. Solids **134**, 103738 (2020).
[14]B. Li, F. Jia, Y.-P. Cao, X.-Q. Feng, and H. Gao, "Surface wrinkling patterns on a core-shell soft sphere," Phys. Rev. Lett. **106**, 234301 (2011).
[15]D. Breid and A. J. Crosby, "Curvature-controlled wrinkle morphologies," Soft Matter **9**, 3624–3630 (2013).
[16]P. Ciarletta, V. Balbi, and E. Kuhl, "Pattern selection in growing tubular tissues," Phys. Rev. Lett. **113**, 248101 (2014).
[17]Y. Yang, H.-H. Dai, F. Xu, and M. Potier-Ferry, "Pattern transitions in a soft cylindrical shell," Phys. Rev. Lett. **120**, 215503 (2018).
[18]G. Abadias, E. Chason, J. Keckes, M. Sebastiani, G. B. Thompson, E. Barthel, G. L. Doll, C. E. Murray, C. H. Stoessel, and L. Martinu, "Review article: Stress in thin films and coatings: Current status, challenges, and prospects," J. Vac. Sci. Technol., A **36**, 020801 (2018).
[19]H. Vandeparre, M. Piñeirua, F. Brau, B. Roman, J. Bico, C. Gay, W. Bao, C. N. Lau, P. M. Reis, and P. Damman, "Wrinkling hierarchy in constrained thin sheets from suspended graphene to curtains," Phys. Rev. Lett. **106**, 224301 (2011).
[20]J. Huang, M. Juszkiewicz, W. H. de Jeu, E. Cerda, T. Emrick, N. Menon, and T. P. Russell, "Capillary wrinkling of floating thin polymer films," Science **317**, 650–653 (2007).
[21]S. D. Janssens, S. Drijkoningen, and K. Haenen, "Ultra-thin nanocrystalline diamond membranes as pressure sensors for harsh environments," Appl. Phys. Lett. **104**, 073107 (2014).
[22]S. D. Janssens, D. Vázquez-Cortés, A. Giussani, J. A. Kwiecinski, and E. Fried, "Nanocrystalline diamond-glass platform for the development of three-dimensional micro- and nanodevices," Diamond Relat. Mater. **98**, 107511 (2019).
[23]O. A. Williams, O. Douhéret, M. Daenen, K. Haenen, E. Ōsawa, and M. Takahashi, "Enhanced diamond nucleation on monodispersed nanocrystalline diamond," Chem. Phys. Lett. **445**, 255–258 (2007).
[24]S. D. Janssens, P. Pobedinskas, J. Vacik, V. Petráková, B. Ruttens, J. D'Haen, M. Nesládek, K. Haenen, and P. Wagner, "Separation of intra- and intergranular magnetotransport properties in nanocrystalline diamond films on the metallic side of the metal–insulator transition," New J. Phys. **13**, 083008 (2011).
[25]A. Kriele, O. A. Williams, M. Wolfer, D. Brink, W. Müller-Sebert, and C. E. Nebel, "Tuneable optical lenses from diamond thin films," Appl. Phys. Lett. **95**, 031905 (2009).
[26]F. Xu, C. Fu, and Y. Yang, "Water affects morphogenesis of growing aquatic plant leaves," Phys. Rev. Lett. **124**, 038003 (2020).
[27]V. Reboud, A. Gassenq, N. Pauc, J. Aubin, L. Milord, Q. M. Thai, M. Bertrand, K. Guilloy, D. Rouchon, J. Rothman, T. Zabel, F. Armand Pilon, H. Sigg, A. Chelnokov, J. M. Hartmann, and V. Calvo, "Optically pumped GeSn microdisks with 16% Sn lasing at 3.1 μm up to 180 K," Appl. Phys. Lett. **111**, 092101 (2017).
[28]A. F. Sartori, P. Belardinelli, R. J. Dolleman, P. G. Steeneken, M. K. Ghatkesar, and J. G. Buijnsters, "Inkjet-printed high-q nanocrystalline diamond resonators," Small **15**, 1803774 (2019).
[29]F. Box, D. O'Kiely, O. Kodio, M. Inizan, A. A. Castrejón-Pita, and D. Vella, "Dynamics of wrinkling in ultrathin elastic sheets," Proc. Natl. Acad. Sci. U. S. A. **116**, 20875–20880 (2019).